1-1-2018

Magnetoelectric Coupling in Nanoscale 0-1 Connectivity

Yan Zong
University of Wollongong, yz818@uowmail.edu.au

Zhilian Yue
University of Wollongong, zyue@uow.edu.au

Pedro M. Martins
University of Minho

Jincheng Zhuang
University of Wollongong, jincheng@uow.edu.au

Yi Du
University of Wollongong, ydu@uow.edu.au

See next page for additional authors

Magnetoelectric Coupling in Nanoscale 0-1 Connectivity

Abstract

The strain-mediated magnetoelectric (ME) coupling between piezoelectric (PE) and magnetostrictive (MS) components are established in various connectivities. Discovering new ME connectivity and elucidating the key factors governing the performance of ME composite are of critical importance to find advanced materials for modern electronics. Reported here is a novel ME coupling in 0-1 connectivity. The unique self-assembling ability of 1-dimension crystalline nanocellulose (CNC) nanowhiskers enables the establishment of ME coupling with 0-dimension cobalt ferrite (CFO) nanoparticles without the use of binder. The developed CFO/CNC 0-1 ME composites display a significant ME voltage coefficient (αME) as high as 0.135 mV cm−1 Oe−1. The CFO nanoparticles are also modified with a cationic surfactant, cetyltrimethylammonium bromide (CTAB), to reduce their dispersion ability. A ME response related to the rearrangement of aggregated MS nanoparticles is observed in the CTAB-CFO/CNC composites, which differs from the typical magnetostriction induced ME effect in nanoparticulate ME composites.

Keywords

connectivity, nanoscale, coupling, magnetoelectric, 0-1

Disciplines

Engineering | Physical Sciences and Mathematics

Publication Details

Zong, Y., Yue, Z., Martins, P., Zhuang, J., Du, Y., Lanceros-Mendez, S. & Higgins, M. J. (2018). Magnetoelectric Coupling in Nanoscale 0-1 Connectivity. Nanoscale, 10 17370-17377.

Authors

Yan Zong, Zhilian Yue, Pedro M. Martins, Jincheng Zhuang, Yi Du, Senentxu Lanceros-Mendez, and Michael J. Higgins

Magnetoelectric Coupling in Nanoscale 0-1 Connectivity†

Yan Zong,[a] Zhilian Yue,[a] Pedro Martins,[b] Jincheng Zhuang,[c] Yi Du,[c] Senentxu Lanceros-Mendez[d,e] and Michael J. Higgins*[a]

[a.] *ARC Centre for Electromaterials Science (ACES), Intelligent Polymer Research Institute/AIIM Faculty, Innovation Campus, Squires Way, University of Wollongong, NSW 2522, Australia.*

[b.] *Centro/Departamento de Física, Universidade do Minho, Braga 4710-057, Portugal.*

[c.] *The Institute for Superconducting and Electronic Materials/AIIM Faculty, Innovation Campus, Squires Way, University of Wollongong, NSW 2522, Australia.*

[d.] *BCMaterials, Basque Center for Materials, Applications and Nanostructures, UPV/EHU Science Park, 48940 Leioa, Spain.*

[e.] *IKERBASQUE, Basque Foundation for Science, 48013 Bilbao, Spain.*

†Electronic Supplementary Information (ESI) available. See DOI: 10.1039/ x0xx00000x

abstract

The strain-mediated magnetoelectric (ME) coupling between piezoelectric (PE) and magnetostrictive (MS) components are established in various connectivities. Discovering new ME connectivity and elucidating the key factors governing the performance of ME composite are of critical importance to find advanced materials for modern electronics. Reported here is a novel ME coupling in 0-1 connectivity. The unique self-assembling ability of 1-dimension crystalline nanocellulose (CNC) nanowhiskers enables the establishment of ME coupling with 0-dimension cobalt ferrite (CFO) nanoparticles without the use of binder. The developed CFO/CNC 0-1 ME composites display a significant ME voltage coefficient (α_{ME}) as high as 0.135 mV cm^{-1} Oe^{-1}. The CFO nanoparticles are also modified with a cationic surfactant, cetyltrimethylammonium bromide (CTAB), to reduce their dispersion ability. A ME response related to the rearrangement of aggregated MS nanoparticles is observed in the CTAB-CFO/CNC composites, which differs from the typical magnetostriction induced ME effect in nanoparticulate ME composites.

Introduction

The magnetoelectric (ME) effect is an elastic coupling interaction between electrical polarization and magnetostrictive components to enable magnetic-to-electrical signal conversion. Early studies on chromium (III) oxide (Cr_2O_3) reported a ME voltage coefficient ~0.01 V Oe^{-1} cm^{-1}, which is the highest value for ME single phase crystals to date.[1] Due to the good ME performance at room temperature,[2, 3] ME composites are promising for a wide range of applications from electronic to magnetic devices.[4, 5] The presence of separated piezoelectric (PE) and magnetostrictive (MS) components that coexist in ME composites can give rise to strain-mediated giant ME responses (>1 V Oe^{-1} cm^{-1}) orders of magnitude higher compared to single phase ME crystals (*e.g.* Cr_2O_3).[6] The elastic connection between the two phases is essentially the tensor property and regarded as the configuration of merit required to produce the enhanced ME coupling[7] and associated output voltage.[3] Thus, studies on various configurations and 'connectivities' between the two phases have attracted extensive research interest.[8]

Generally, the connectivity of ME coupling is determined according to the dimension of the MS and PE phases. In particular, particulate composites consisting of MS particles within a bulk PE material is known as 0-3 connectivity,[9-11] laminate composites comprising MS and PE layers are in a 2-2 connectivity,[12-14] and heterostructural composites with MS rods embedded in a PE bulk are defined as 1-3 connectivity.[15-18] These aforementioned connectivities are well-studied however novel connectivities are emerging and being explored for their ME properties. For example, a significant increase in the non-resonant ME effect with α_{ME} of 22 V Oe^{-1}

cm^{-1} was achieved using a composite in 2-1 connectivity; this consists of a layer of aligned PE fibers (1-D) laminated with a Metglas layer (2-D).[1] A novel 1-1 connectivity ME composite consisting of a $Pb(Mg,Nb)O_3$-$PbTiO_3$ (PMN-PT) single-crystal fiber (1-D) combined with a Metglas fiber (1-D) showed a dramatic enhancement of the α_{ME} with a value of ~7,000 V Oe^{-1} cm^{-1} at resonance, which is approximately 7 times higher than the previously studied 2-1 connectivity PMN-PT piezofiber layer/Metglas composite.[19] Ceramic nanoparticles/wires are typically used to produce particulate composites to achieve connectivities of 0-0 or 0-1 however due to the poor adhesive property of ceramic-based nanoparticles or nanowires an additional component such as polymer binder is required to build up ME coupling via elastic polymer bulk. Earlier studies involve the use of polymer as a binder (3-D bulk) to provide strain coupling between MS (0-D) and PE (0-D) nanoparticles.[20, 21] These ME composite consisting of three phases are not considered to be 0-0 type but effectively 0-0-3 in connectivity. Therefore, in order to achieve a purely two phase ME composite in 0-0 or 0-1 connectivities at least one of the two phases should be a self-assembling material to enable the formation of stable composites, *e.g.* consisting of 2 different MS and PE nanomaterials without a binder.

Crystalline nanocellulose (CNC) nanowhisker as a 1-D, high aspect ratio,[22] PE material is very suitable to fabricate novel connectivity ME composites. They have self-assembly properties,[23] thus providing the possibility of developing a two-phase composite with embedded magnetic nanoparticles,[24, 25] to enable ME coupling in low-dimension 0-1 connectivity.

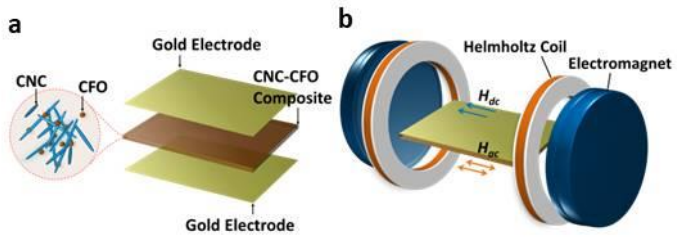

Fig 1. (a) Schematic view of CNC embedded MS nanoparticles composite and the ME coupling in nanoscopic 0-1 connectivity. (b) Schematic view of the bulk system for ME voltage measurement. The output voltage was collected from the interface gold electrodes and monitored as root mean square (RMS) values using a lock-in amplifier.

In this work, we develop the first 0-1 connectivity ME composites based on CNC. To achieve this, MS nanoparticles were embedded in a cellulose nanowhisker network whereby the nanoparticle diameter and CNC nanowhiskers width were both on the scale of nanometers and therefore the ME coupling between the two components were considered to be a nanoscopic 0-1 connectivity (Fig. 1a). The physical mechanism model of the ME composites can be expressed as: ME composites = MS nanoparticles + PE nanowhiskers. The combination of MS and PE phases give rise to ME effect (an output voltage) and occurs to strain transfer from the MS phase to the PE phase. Some physical experiment analysis, *e.g.* X-ray diffraction (XRD) and magnetic hysteresis, was employed to confirm the properties of the PE and MS phases, as well as the coexistence of the two phases. The ME effect of the developed composites was studied using a dynamic measuring method (Fig. 1b) (details can be

found in experimental section).[26] To study the effect of elastic coupling interaction between the PE and MS nanomaterials, two types of MS nanoparticles, namely cobalt ferrite (CFO) and surfactant modified CFO with cetyltrimethylammonium bromide (CTAB-CFO) were employed. CNC produced from sulfuric acid hydrolysis presents surface sulfonic groups, and both CNC and CFO possess hydroxyl groups. Consequently, their hydrophilic surfaces were conducive to the formation of hydrogen bonding, enabling a relatively stable interaction between the CNC and CFO. In contrast, CTAB-CFO nanoparticles were more hydrophobic and expected to form a weaker interaction with the CNC due to the reduced hydrogen bonding.

Results and Discussion

Morphology and Crystallinity of CNC Nanowhiskers

CNC can be produced from different resources and among them CNC synthesized from cotton were high crystalline products with crystallinity >85 %.[23, 27, 28] The CNC nanowhiskers used for this work were synthesized from filter paper, which contained 100% cotton α-cellulose. The obtained CNC nanowhiskers have high aspect ratio, with ~300 nm in length and 40-60 nm in width (Fig. 2a). XRD (Fig. 2b) spectrum reveals the nanowhiskers retain the cellulose I crystalline lattice of the cotton α-cellulose before acid hydrolysis,[29] indicating that the synthesis process does not affect the crystalline configuration. Previously our group found that the cellulose crystallinity plays a direct role in the PE properties and further influences the ME effect.[30] As such, synthesizing and/or treating cellulose to induce a higher degree of crystallinity is expected to increase performance of ME composite output voltages. Different methods were reported to study the crystallinity of cellulose[29, 31] and the crystallinity index (DI) calculated from XRD intensity is one of the most reliable methods, which is expressed by the following equation:[29]

$$CI = \frac{(I_{002} - I_{am})}{I_{002}} \quad (1)$$

where I_{002} is the intensity of (002) peak at 22.82˚ and I_{am} is the intensity of the amorphous component at 2ϑ of 18˚ for cellulose crystalline I (Fig. 2b).[29] Based on equation 1 the CI of CNC in this study is calculated as 91.72%, which is slightly higher than previously reported CNC nanowhiskers synthesized from cotton.[27]

PE Properties of CNC Nanowhiskers

As the only suitable technique that allows PE measurement on nanomaterials, Switching Spectroscopy-Piezoresponse Force Microscopy (SS-PFM) was used to measure the local, nanoscale PE properties. The dynamic of the CNC nanowhisker piezoresponse was confirmed as hysteresis loops in both displacement (change in amplitude) and phase signals as a function of the applied tip voltage (Fig. 2c). A classical butterfly shape of the displacement and 180˚ change in the phase confirms a fully reversible PE dynamic, which is explained by the bias-induced di-polarization process of a PE material.[32-34] The amplitude displacement at positive biases regime (10~25V) is less than that at negative biases regime (-10~-25V), resulting in larger left wing of the butterfly loops in comparison to the right wing. This unique PE dynamic was also observed in our earlier work on regenerated cellulose, indicating cellulose's amplitude displacement is more sensitive to negative biases stimulation.[30] This phenomenon is probably related to the surface charge or the polarization orientation of cellulose matrix, however the essential mechanism remains unreported. Based on a tip bias induced displacement and a coercive field of approximately 38 V (from -18 to over 20 V), the PE coefficient is estimated to be 11.67 ± 0.94 pm V^{-1} resulting from an average of three hysteresis loops based on three testing points, and is similar to CNC whiskers produced from α-cellulose powder in previous work.[35]

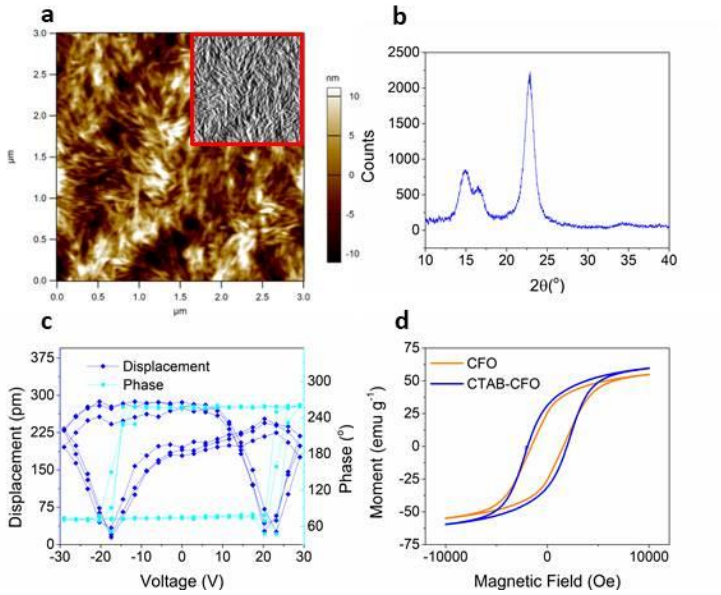

Fig 2. (a) AFM height and phase images (inset section) of cellulose nanowhiskers, the scanning size is 3 μm ×3 μm. (b) XRD spectrum of the resulted CNC. The cellulose nanowhiskers have interference rising at diffraction angles 2θ=14.9˚, 17.4˚, 20.7˚, 22.8˚ and 34.6˚ corresponding to lattice (101), (10$\tilde{1}$), (021), (002) and (004), which is the typical XRD spectrum for cellulose crystalline I. (c) The hysteresis loops (3 cycles) representing the bias induce amplitude displacement as well as the phase changes corresponding to the displacement hysteresis loops. (d) Magnetic hysteresis loops of CFO and CTAB-CFO nanoparticles measured at room temperature (300K).

Magnetic Properties of CFO and CTAB-CFO Nanoparticles

Fig. 2d show the magnetic hysteresis loops of CFO and CTAB-CFO nanoparticles, respectively. The particle size of the commercial CFO was ~30 nm as indicated by the supplier and the CTAB-CFO was ~50 nm.[36] The saturation magnetization values under room temperature were 54.79 emu g^{-1} for CFO and 59.72 emu g^{-1} for CTAB-CFO nanoparticles, both of which were slightly lower than the values obtained previously for 24 nm sized CFO sample.[37] However, an obvious difference was found in their coercivity values, which were 3200 Oe and 3870 Oe for CFO and CTAB-CFO nanoparticles, respectively, and in contrast to 1205 Oe for the 24 nm sized CFO sample.[37] The wider coercive fields of CFO and CTAB-CFO nanoparticles in this work were presumably caused by their increased volume, a finding also observed in spherical and cubic CFO nanocrystals at extremely low temperature of 5K.[38]

Dispersion Properties of CFO and CTAB-CFO Nanoparticles

Unlike nanoparticulate 0-3 ME composites in which nanoparticles are embedded in a soft polymer bulk,[39, 40] the CFO and CTAB-CFO nanoparticles were distributed in a matrix consisting of only CNC nanowhiskers. To

understand the effect of magnetic nanoparticle surface chemistry, such as hydrophilic and hydrophobic groups, on their physical interactions with CNC nanowhiskers and subsequently on the ME composite properties, hydrophilic CFO nanoparticles and hydrophobically modified CTAB-CFO nanoparticles were investigated. The effect of surface groups on magnetic nanoparticle dispersions in aqueous condition is shown in ESI Fig. S1a,b. Both CFO and CTAB-CFO nanoparticles showed good dispersions in DI water after sonication (ESI Fig. S1a). After standing for 10 min, the CFO nanoparticles maintained their stable suspension, however most of the CTAB-CFO nanoparticles precipitated in aggregated form (ESI Fig. S1b). A CNC suspension (CNC mass is equivalent to MS nanoparticles) was then added to the nanoparticle dispersions, followed by sonication (ESI Fig. S1c). In this case, CNC is a hydrophilic nanomaterial due to the presence of surface hydroxyl groups, in addition to sulfonic groups from the acid hydrolysis process, that enable the formation of stable aqueous dispersions. Consequently, the hydrophilic CFO nanoparticles with CNC nanowhiskers maintain good dispersions after 12 h whereas in contrast the hydrophobic CTAB-CFO nanoparticles do not maintain dispersions after the same time (ESI Fig. S1d). Over prolonged period of storage (1 week) the CFO nanoparticles with CNC nanowhiskers precipitated (ESI Fig. S1e), most likely due to the magnetic attraction of CFO nanoparticles that reduced the dispersion ability of cellulose nanowhiskers. This suggests the CFO nanoparticles were attached to the CNC nanowhiskers.

Appearance and Characterizations of 0-1 Connectivity ME Composites

The 0-1 connectivity ME composites (2.5 cm × 3.5 cm) were prepared from the mixed dispersions containing different weight ratio percentage concentrations of MS nanoparticles (5, 10 or 20 wt%) (ESI Fig. S2). The composites produced rigid films and their transparency was dependent on the CFO or CTAB-CFO concentrations (ESI Fig. S2). To avoid cracking of the composite films, Al^{3+} ions were introduced to stabilize the CNC network. However, it was found that cracking/breaking could not be avoided if the MS nanoparticles were over 25 wt%, as shown in ESI Fig. S3.

The crystalline structure of the developed composites was investigated using XRD. Representative spectra of CFO/CNC and CTAB-CFO/CNC composites containing 20 wt% MS nanoparticles (black curves) in comparison with pure CFO and CTAB-CFO nanoparticles (red curves) are displayed in Fig. 3a,b. The interference of CFO and CTAB-CFO nanoparticles showed good agreement with previously reported indices of cobalt ferrite,[41] and no impurities were observed in the spectra. Spectra of the 0-1 connectivity ME composites (CFO/CNC and CTAB-CFO/CNC) show the interference of CNC in the range from 13˚-25˚ combined with the characteristic peaks of the pure CFO and CTAB-CFO nanoparticles at diffraction angles from 30˚-65˚, confirming the coexistence of PE and MS phases in the composites. The interference indices corresponding to the cellulose lattice (004) at 34.6˚ and CFO lattice (111) at 19.9˚ have low intensity and therefore were not observed in spectra of the composites. FT-IR spectra of pure CNC (Fig. 3c,d) and the composites containing 5, 10, 20 wt% CFO (Fig. 3c) and CTAB-CFO (Fig. 3d) nanoparticles showed a series of absorption bands at 985, 1000 and 1015 cm^{-1}, which were all assigned to cellulose C-O stretching.[42] These bonds suggested a static interaction between MS particles and CNC nanowhiskers, however the underlying mechanism is yet to be elucidated.

Surface Morphology of 0-1 Connectivity ME Composites

AFM was used to study the surface morphology of 0-1 connectivity ME composites containing 20 wt% of MS nanoparticles. AFM height images showed a relatively smooth surface for CFO/CNC composite composites with the appearance of some particulate regions (ESI Fig. S4a) although no clear observations of individual CFO nanoparticles were made when the scan size was reduced to 3 µm and only the CNC whiskers were observed (ESI Fig. S4b). Surface roughness was calculated based over 15 µm images (ESI Fig. S4a and c), giving low values (RMS = 9.34 nm) attributed to the good dispersion ability of CFO nanoparticles. In contrast, significantly more

particulate regions were observed on the CTAB-CFO/CNC, with greater surface roughness with RMS = 80.34 nm, that may be due to surface aggregated MS nanoparticles (ESI Fig. S4c). Higher resolution images showed the presence of these aggregations on the CNC nanowhiskers surface (ESI Fig. S4d).

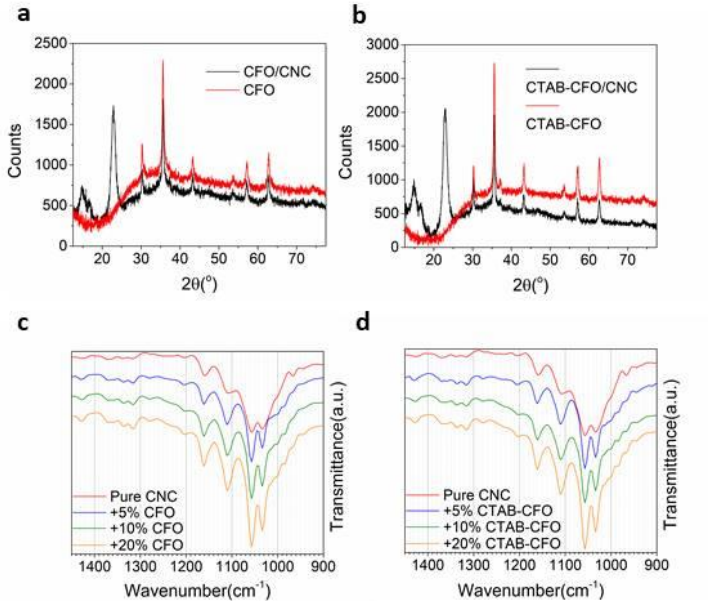

Fig 3. XRD patterns of (a) CFO nanoparticles and CFO/CNC composite and (b) CTAB-CFO nanoparticles and CTAB-CFO/CNC composite. The CFO/CTAB-CFO have interference rising at diffraction angles 2θ=18.5˚, 30.2˚, 35.6˚, 36.3˚, 43.3˚, 53.8˚, 57.2˚, 62.8˚ and 74.1˚ corresponding to lattice (111), (220), (311), (222), (400), (422), (511), (440) and (533). (c, d) FT-IR spectra of pure CNC and (c) CFO/CNC and (d) CTAB-CFO/CNC composites containing different weight ratios of MS particles.

ME Effect of 0-1 Connectivity Composites

The ME composites were coated with surface electrodes on both sides (Fig. 1a) and the ME measurements were performed using a dynamic method with an applied alternating magnetic field (H_{ac}) superimposed on a constant magnetic field (H_{dc}) to induce the ME output voltage (Fig. 1b). Based on this method, the ME voltage coefficient is evaluated using the following equation:[43]

$$\alpha_{\mathrm{ME}} = \frac{V_{\mathrm{ME}}}{t \times H\mathrm{ac}} \qquad (2)$$

where V_{ME} is the actual voltage output collected from surface electrodes, t is the thickness of nanocomposite film and H_{ac} is the strength of the alternating magnetic field. The thickness of the CFO/CNC and CTAB-CFO/CNC composites were in the range of 50-60 and 70-80 µm, respectively. The actual magnetic induced output voltages (µV) are given in ESI Fig. S5.

The bulk testing of the ME effect followed the method for previously reported nanoparticulate CFO/P(VDF-TrFE) ME composites: for all measurements, H_{ac} was settled at 0.6 Oe with fixed frequency of 5 kHz.[40, 44] It is known a resonance enhanced ME effect occurs in laminated composites: when the frequency of inducing H_{ac} encounters the inherent frequency of MS layer the strain is amplified thus the output voltage reaches the peak value.[45] The electromagnetic resonance (f_r) corresponding to the enhanced ME response is determined by the physical properties of the MS layer, including its density (ρ), Young's modulus (E) and the length (L) along the magnetic field:

$$f_r = 1/2L \times \sqrt{E/\rho} \tag{3}$$

However in nanoparticulate composites no obvious frequency enhanced ME effect can be observed due to variation of the MS particle sizes and the tendency to form aggregated form of nanoparticles. As such, only the ME effect dependence on H_{dc} values were elucidated in this study. In particular, the ME output voltage was recorded using a lock-in amplifier (see details in method section) and the α_{ME} was calculated according to gradually increased H_{dc} strength and. Fig. 4 show that no clear ME response was observed for CFO/CNC and CTAB-CFO/CNC composites containing 5 wt% of magnetic nanoparticles, most likely due to insufficient magnetostriction to induce strain required for a measurable ME effect. At higher concentrations of MS nanoparticles, a ME effect is observed with composites containing

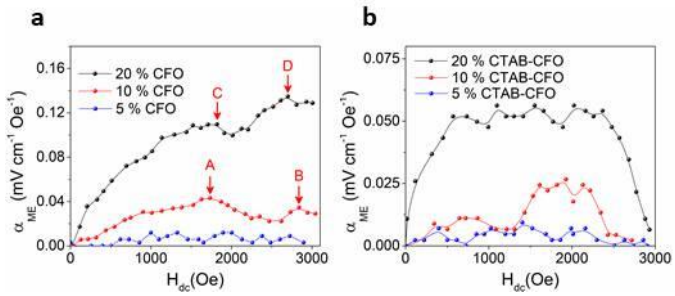

Fig 4. α_{ME} as a function of H_{dc} for (a) CFO/CNC and (b) CTAB-CFO/CNC composites with MS concentrations of 5, 10 and 20 wt%. For all experiments H_{ac} was 0.6 Oe and the frequency was fixed at 5 kHz. For allexperiments H_{ac} was 0.6 Oe and the frequency was fixed at 5 kHz.

20 wt% MS nanoparticles giving a higher α_{ME} value compared to those with 10 wt% concentration regardless of the type of MS nanoparticles (Fig. 4). Generally, because the MS nanoparticles are well dispersed in the system, the CFO/CNC composites have a similar α_{ME}-H_{dc}dependent behavior, as previously shown for CFO/P(VDF-TrFE) composites; the α_{ME} gradually increased according to H_{dc} from 0 to approximately 2000 Oe. Such behavior is explained by the increase of the effective piezo-magnetic coefficient until the optimum H_{dc} is reached.[46] After ~3000 Oe, a decay in α_{ME} was observed as previously described for CFO/P(VDF-TrFE) composites resulted by a reduced magnetostriction of CFO nanoparticles after saturation status.[40, 44] Due to the limitation of our ME testing system the α_{ME} could not be recorded beyond 3000 Oe. Specifically, α_{ME} from 10 wt% CFO/CNC composites (Fig. 4a, red trace) gradually increases until peaking at ~1800 Oe (Point A, 0.039 mV cm^{-1} Oe^{-1})

followed by a second peak at ~2838 Oe (Point B, 0.038 mV cm^{-1} Oe^{-1}). For the 20 wt% CFO/CNC composites (Fig. 4a, black trace), again the α_{ME} gradually increases with an increase in H_{dc}, consisting of two similar peaks of 0.110 mV cm^{-1} Oe^{-1} (Point C) at 1819 Oe and 0.135 mV cm^{-1} Oe^{-1} (Point D) at 2700 Oe (Figure 4a, black trace). The first peak is suggested to be associated with MS properties of CFO nanoparticles of which the saturation is achieved at ~2000 Oe and in good agreement with previously studied particulate ME composites.[40, 44] The second peak is presumably related to the movement of CNC nanowhiskers. As discussed earlier, due to the hydrophilic surfaces CFO nanoparticles can attach to CNC nanowhiskers *via* hydrogen bonding to establish a stable interaction. Driven by the magnetic force, it is possible when H_{dc} reached a threshold value part of the CFO attached CNC nanowhiskers begin to move (ESI Scheme 1), and this movement therefore provided the strain to induce a ME effect giving rise to the second peak. Also, due to the lower CFO concentration, the movement in the 10 wt% sample presumably occurred to a smaller extent in comparison to the 20 wt% sample, as evidenced by the lower second peak value of the 10 wt% sample which occurred at higher H_{dc} strength. The CTAB-CFO/CNC composites, however, showed a different α_{ME}-H_{dc} dependent relationship; the α_{ME} sharply increased to a plateau of 600~2500 Oe for the 20 wt% sample, or plateau of 1500~2300 Oe for the 10 wt% sample (Fig. 4b). For both concentrations, the ME effect reduced dramatically after the magnetic saturation at ~2000 Oe and eventually records zero at the maximum H_{dc} of 3000 Oe (Fig. 4b). Considering the poor dispersion conditions of CTAB-CFO nanoparticles, we interpret the ME response of the CTAB-CFO/CNC composites to be primarily caused by the movement/rotation of aggregated nanoparticles rather than the typical magnetostriction behavior. This is because the aggregated nanoparticles are weakly connected to CNC nanowhiskers and once a strong external magnetic field is applied, the nanoparticle can rearrange and the movement/rotation then provided the strain for an apparent ME voltage output. For the higher concentrated sample (20 wt%) the strain was sufficient to induce an ME response at low H_{dc} and reached the plateau at 600 Oe (Fig. 4b, black trace). The 10 wt% concentrated sample, on the other hand, were not able to produce enough strain to induce measurable ME response until 1300 Oe (Fig. 4b, red trace). When the rearrangement of CTAB-CFO nanoparticles was completed at ~2300 Oe, the α_{ME} sharply dropped to ~0. Compared to the typical magnetostriction induced ME response in nanoparticulate composites, the movement/rotation induced voltage changed faster at both initiation and decay stages, however the corresponding ME voltage is much lower. As evidenced that CFO/CNC composites showed better overall performance, with peak ME values of 0.55 and 0.15 μV for 20 wt% and 10 wt%, respectively (ESI Fig. S5a and c), in comparison to CTAB-CFO/CNC (0.25 and 0.12 μV) (ESI Fig. S5b and d). The concentrations of 5 wt% CFO and CTAB-CFO were two low to induce an ME effect and the recorded voltage in the range of 0-0.05 μV was in the background noise of the measurement (ESI Fig. S5e,f). Also due to the relatively low ME output voltage of CTAB-CFO/CNC composite, the background noise was possibly observed in the corresponding 10 and 20 wt% samples as the small multiple peaks though the exact reason is unclear at this stage.

Conclusion

In conclusion, an ME coupling in 0-1 connectivity was proposed and has been successfully verified in this work. To the best of our knowledge, this is the first ME composite with 0-1 connectivity. Strong hydrogen bonding between the hydrophilic surfaces of CFO and CNC improved the dispersion of MS nanoparticles and gave rise to the highest α_{ME} of 0.135 mV cm^{-1} Oe^{-1} in a CFO/CNC ME composite with the highest MS concentration of 20 wt%. The ME response of CFO/CNC or CTAB-CFO/CNC composites is not as high as PVDF based particulate ME composites in 0-3 connectivity,[44] which is due to the limited PE property of cellulose. Compared to ME laminates which usually generate a giant ME effect of α_{ME}>1 V cm^{-1} Oe^{-1}, the ME voltage of 0-1 connectivity ME composites is relatively low. This is mainly due the structural merit of 2-2 connectivity of ME laminate required for strain

transfer.[45] However, the work provides a new concept for novel ME coupling connectivity and opens up the possibility of using different types of combinations of low-dimension MS and PE materials, for example using 0-D magnetic alloy nanoparticles or 1-D magnetic alloy nanowires with 1-D cellulose nanofibers,[47-49] to investigate ME composites in future.

Experimental Details

CNC Preparation: CNC was produced from filter paper *via* acid hydrolysis using 65 wt% H_2SO_4. To prepare cellulose nanowhiskers, 4g filter paper (Advantec, Lot No. 90909520) was cut into strips 0.5 cm in width and blended with 30 mL H_2SO_4. The hydrolysis reaction took place under 70 ˚C with constant stirring over 1,000 rpm for 20 min. To cease the reaction, 250 mL iced DI water was added and the resultant suspension was washed by centrifugation at ~10,000 rpm for several rounds until the upper layer became turbid. The pH value under this condition is ~ 2. The obtained CNC formed a gel-like aqueous dispersion with concentration of approximately 7 wt%. After calculating the precise concentration of each batch by solvent evaporation method, the CNC samples were stored under 4 ˚C without further treatment until use.

Fabrication of ME Composites: Two types of MS nanoparticles were used to fabricate ME composites. The commercial available CFO nanoparticles (Sigma-Aldrich, Cat. No. 773352) were used as received; the preparation of surfactant modified CTAB-CFO nanoparticles can be found in an earlier study.[36] Firstly, 0.05 g CFO or CTAB-CFO nanoparticles were dispersed in 1.5 mL DI water and sonicated for 0.5 h. The desired amount of CNC suspension was then added to make aqueous dispersions with CNC:CFO (or CNC:CTAB-CFO) in 1:19, 1:9 and 1:4 in weight, and the corresponding MS concentrations in composites were calculated as 5 wt%, 10 wt% and 20 wt%, respectively. To avoid CNC degradation, the dispersions were sonicated for 15 min in an ice bath and poured into Teflon evaporation wells with 0.8 mm in thickness. After evaporation for 2 h, the evaporation wells were immersed in 0.5 M $AlCl_3$ solution for 5 min, followed by DI water washing and dried as films under room temperature (20 ˚C). The ME composite films were further vacuum dried under 50 ˚C to eliminate residual water and sputter coating used to deposit 30 nm gold layers as surface electrodes for the ME measurements (Fig.1a).

Bulk ME Effect Measurement: An alternating Helmholtz coil was used to apply a magnetic ac field at 0.6 Oe at a fixed frequency of 5 kHz following the method in previous report.[44] A separate electromagnet was use to apply magnetic dc fields with strengths in the range of 0-3000 Oe and both the ac and dc magnetic fields were applied simultaneously along the length direction of the ME laminate composites (Fig. 1b). The induced ME output voltage was recorded using a model SR8 10 DSP lock-in amplifier.

Magnetic Measurement: Magnetic properties of CFO and CTAB-CFO nanoparticles were characterized using a 14T PPMS system with vibrating sample magnetometer (VSM) function. All measurements were taken under room temperature (300K) with applied magnetic fields ranging from -10,000 to 10,000 Oe.

X-Ray Diffraction (XRD): XRD measurements were performed on CNC using a GBC MMA XRD (λ = 1.54Å) in the range of 10-80 ˚ on the 0-1 connectivity ME composite films and CFO/CTAB-CFO nanoparticles. The voltage, current and scanning speed were set to −40 kV, 25mA and 2˚ min^{-1}, respectively.

Fourier Transform Infrared Spectroscopy (FT-IR): FT-IR spectrum was recorded on a Shimadzu AIM8000 FT-IR spectrometer. The pure CNC film and the 0-1 connectivity ME composite films were measured using an FT-IR attenuated total reflectance (ATR) method in the range of 900-1450 cm^{-1}.

Atomic Force Microscope (AFM): An MFP-3D Atomic Force Microscope (Asylum Research, Santa Barbara, US) was used for imaging the CNC, magnetic nanoparticles and 0-1 ME composite films. AFM imaging was performed using a Tap300-G tip (Budget Sensors, Bulgaria) with resonant frequency of 300 kHz and spring constant of 40 N m^{-1}. The height and phase images were obtained in air using tapping mode with scan rate of 1.0 Hz.

Piezoresponse Force Microscopy (PFM): The local PE response of CNC was measured with an MFP-3D Atomic Force Microscope (Asylum Research, Santa Barbara, US) using PFM. A conductive tip (Olympus OMCL-AC240TM) with Pt/Ti coating, resonant frequency of 70 kHz and spring constant of ~2.0 N m^{-1} were used. The PFM height, amplitude and phase images were obtained in Dual AC Response Tracking (DART) mode[50] with contact resonant frequency of ~ 260 kHz. The PE response was measured as the first-harmonic of a bias-induced tip deflection: $d = d_0 + A\cos(\omega t + \varphi)$, where d_0 is the equilibrium position of the tip; A is the amplitude and ω is the frequency of applied bias; φ is the phase yielded information on the polarization direction below the tip. To study the polarization switching dynamics, switching spectroscopy-PFM (SS-PFM) was used to obtain the local PE hysteresis loop. For each laminate sample, SS-PFM measurements were acquired across a 3 × 3 μm^2 area by applying a bias at least 5 positions on the sample. The voltage during the SS-PFM measurements was applied in the range of ±29 V with a frequency of 0.5 Hz, which was sufficient to reversibly switch the polarization component. To enable this, the PFM instrumentation was modified by connecting an external amplifier to increase the upper limit of output signal to ±30 V. The driving amplitude was set to 200 mV for all PFM measurements. To perform the SS-PFM measurements, the CNC nanowhiskers were drop cast onto a gold mylar substrate, and then a sequence of inducing bias is applied through a conductive tip. To estimate the PE coefficient, the peak value of displacement was divided by the corresponding inducing bias based on three testing points.

Conflicts of interest

The authors declare no conflicts of interest.

References

1. S. Dong, J. Zhai, J. Li and D. Viehland, *Applied Physics Letters*, 2006, **89**, 252904.
2. W. Eerenstein, N. Mathur and J. F. Scott, *nature*, 2006, **442**, 759-765.
3. N. A. Spaldin and M. Fiebig, *Science*, 2005, **309**, 391-392.
4. C.-W. Nan, M. I. Bichurin, S. Dong, D. Viehland and G. Srinivasan, *Journal of Applied Physics*, 2008, **103**, 031101.
5. J.-M. Hu, L.-Q. Chen and C.-W. Nan, *Advanced Materials*, 2016, **28**, 15-39.
6. J. Ma, J. Hu, Z. Li and C.-W. Nan, *Advanced Materials*, 2011, **23**, 1062-1087.
7. J. V. Suchtelen, *Philips Research Reports*, 1972, **27**, 28-37.
8. H. Palneedi, V. Annapureddy, S. Priya and J. Ryu, *Actuators*, 2016, **5**, 9.
9. Y. Li, Z. Wang, J. Yao, T. Yang, Z. Wang, J.-M. Hu, C. Chen, R. Sun, Z. Tian, J. Li, L.-Q. Chen and D. Viehland, *Nature Communications*, 2015, **6**, 6680.
10. R. A. Islam, V. Bedekar, N. Poudyal, J. P. Liu and S. Priya, *Journal of Applied Physics*, 2008, **104**, 104111.
11. M. Etier, V. V. Shvartsman, S. Salamon, Y. Gao, H. Wende and D. C. Lupascu, *Journal of the American Ceramic Society*, 2016, **99**, 3623-3631.
12. R. A. Islam, Y. Ni, A. G. Khachaturyan and S. Priya, *Journal of Applied Physics*, 2008, **104**, 044103.

13. Y. Wang, D. Gray, D. Berry, J. Gao, M. Li, J. Li and D. Viehland, *Advanced Materials*, 2011, **23**, 4111-4114.
14. J. Ryu, S. Priya, A. V. Carazo, K. Uchino and H.-E. Kim, *Journal of the American Ceramic Society*, 2001, **84**, 2905-2908.
15. J. Ma, Z. Shi and C. W. Nan, *Advanced Materials*, 2007, **19**, 2571-2573.
16. K. H. Lam, C. Y. Lo and H. L. W. Chan, *Journal of Applied Physics*, 2010, **107**, 093901.
17. Z. Shi, C.-W. Nan, J. Zhang, J. Ma and J.-F. Li, *Journal of Applied Physics*, 2006, **99**, 124108.
18. Y. Bai, N. Jiang and S. Zhao, *Nanoscale*, 2018, **10**, 9816-9821.
19. Z. Chu, H. Shi, W. Shi, G. Liu, J. Wu, J. Yang and S. Dong, *Advanced Materials*, 2017, **29**, 1606022.
20. C.-W. Nan, L. Liu, N. Cai, J. Zhai, Y. Ye, Y. H. Lin, L. J. Dong and C. X. Xiong, *Applied Physics Letters*, 2002, **81**, 3831-3833.
21. K. H. Chau, Y. W. Wong and F. G. Shin, *Applied Physics Letters*, 2009, **94**, 202902.
22. J. P. F. Lagerwall, C. Schutz, M. Salajkova, J. Noh, J. Hyun Park, G. Scalia and L. Bergstrom, *NPG Asia Mater*, 2014, **6**, e80.
23. Y. Habibi, L. A. Lucia and O. J. Rojas, *Chemical Reviews*, 2010, **110**, 3479-3500.
24. S.-L. Cao, X.-H. Li, W.-Y. Lou and M.-H. Zong, *Journal of Materials Chemistry B*, 2014, **2**, 5522-5530.
25. E. Lizundia, A. Maceiras, J. L. Vilas, P. Martins and S. Lanceros-Mendez, *Carbohydrate Polymers*, 2017, **175**, 425-432.
26. G. V. Duong, R. Groessinger, M. Schoenhart and D. Bueno-Basques, *Journal of Magnetism and Magnetic Materials*, 2007, **316**, 390-393.
27. B. Sun, M. Zhang, Q. Hou, R. Liu, T. Wu and C. Si, *Cellulose*, 2016, **23**, 439-450.
28. D. Trache, M. H. Hussin, M. K. M. Haafiz and V. K. Thakur, *Nanoscale*, 2017, **9**, 1763-1786.
29. M. L. Nelson and R. T. O'Connor, *Journal of Applied Polymer Science*, 1964, **8**, 1325-1341.
30. Y. Zong, T. Zheng, P. Martins, S. Lanceros-Mendez, Z. Yue and M. J. Higgins, *Nature Communications*, 2017, **8**, 38.
31. L. Segal, J. J. Creely, A.E. Martin, Jr. and C. M. Conrad, *Textile Research Journal*, 1959, **29**, 786-794.
32. S. Jesse, A. P. Baddorf and S. V. Kalinin, *Applied Physics Letters*, 2006, **88**, 062908.
33. M. J. Polking, M.-G. Han, A. Yourdkhani, V. Petkov, C. F. Kisielowski, V. V. Volkov, Y. Zhu, G. Caruntu, A. Paul Alivisatos and R. Ramesh, *Nauret Materials*, 2012, **11**, 700-709.
34. G. Caruntu, A. Yourdkhani, M. Vopsaroiu and G. Srinivasan, *Nanoscale*, 2012, **4**, 3218-3227.
35. Y. Zong, Z. Yue and J. Higgins Michael, *Macromolecular Materials and Engineering*, 2018, **303**, 1800099.
36. P. Martins, C. Caparros, R. Gonçalves, P. M. Martins, M. Benelmekki, G. Botelho and S. Lanceros-Mendez, *The Journal of Physical Chemistry C*, 2012, **116**, 15790-15794.
37. K. Maaz, A. Mumtaz, S. K. Hasanain and A. Ceylan, *Journal of Magnetism and Magnetic Materials*, 2007, **308**, 289-295.
38. Q. Song and Z. J. Zhang, *Journal of the American Chemical Society*, 2004, **126**, 6164-6168.
39. C. W. Nan, M. Li and J. H. Huang, *Physical Review B*, 2001, **63**, 144415.
40. J. X. Zhang, J. Y. Dai, L. C. So, C. L. Sun, C. Y. Lo, S. W. Or and H. L. W. Chan, *Journal of Applied Physics*, 2009, **105**, 054102.
41. V. Pillai and D. O. Shah, *Journal of Magnetism and Magnetic Materials*, 1996, **163**, 243-248.
42. C. Y. Liang and R. H. Marchessault, *Journal of Polymer Science*, 1959, **39**, 269-278.
43. S. Reis, M. P. Silva, N. Castro, V. Correia, J. G. Rocha, P. Martins, A. Lasheras, J. Gutierrez and S. Lanceros-Mendez, *Smart Materials and Structures*, 2016, **25**, 085028.

44. P. Martins, A. Lasheras, J. Gutierrez, J. M. Barandiaran, I. Orue and S. Lanceros-Mendez, *Journal of Physics D: Applied Physics*, 2011, **44**, 495303.
45. G. Srinivasan, *Annual Review of Materials Research*, 2010, **40**, 153-178.
46. P. Martins, Y. V. Kolen'ko, J. Rivas and S. Lanceros-Mendez, *ACS Applied Materials & Interfaces*, 2015, **7**, 15017-15022.
47. P. D. McGary and B. J. H. Stadler, *Journal of Applied Physics*, 2005, **97**, 10R503.
48. T. Saito, Y. Okita, T. T. Nge, J. Sugiyama and A. Isogai, *Carbohydrate Polymers*, 2006, **65**, 435-440.
49. E. V. Shevchenko, D. V. Talapin, H. Schnablegger, A. Kornowski, Ö. Festin, P. Svedlindh, M. Haase and H. Weller, *Journal of the American Chemical Society*, 2003, **125**, 9090-9101.
50. J. R. Brian, C. Clint, V. K. Sergei and P. Roger, *Nanotechnology*, 2007, **18**, 475504.